 doi:10.20944/preprints202206.0187.v1

Article

Generalization and Expansion of the Hermia Model for a Better Understanding of Membrane Fouling

Gustavo Pereira [1,*], Lucio Cardozo-Filho[1,2], Veeriah Jegatheesan[2] and Reginaldo Guirardello[3]

[1] Department of Chemical Engineering, State University of Maringa, Maringa, Brazil
[2] School of Engineering and Water: Effective Technologies and Tools (WETT) Research Centre, RMIT University, Melbourne, VIC 3000, Australia
[3] College of Chemical Engineering, State University of Campinas, Campinas, Brazil
* Correspondence: gldpereira2@gmail.com; Tel.: +55 44 99182 8901

Abstract: One of the most broadly used models for membrane fouling is the Hermia model, which separates this phenomenon into four blocking mechanisms, each with an associated parameter n. These mechanisms are complete blocking ($n = 2$), intermediate blocking ($n = 1$), standard blocking ($n = 3/2$) and cake formation ($n = 0$). The original model, which was obtained through experimental data, is given by an Ordinary Differential Equation (ODE) dependent on n. At the time, this ODE was only solved for these four values of n, which limits the effectiveness of the model when adjusted to experimental data. The aim of this paper is to not only mathematically prove the original Hermia model, but also to broaden the scope of this model for any real number n by using the original ODE, the equations of fluid mechanics and the properties of single and multivariable calculus. The final generalized Hermia model is given by a power-law for any $n \neq 2$ and is given by an exponential function at $n = 2$ and can be fitted to ultrafiltration, microfiltration, nanofiltration and reverse osmosis data with acceptable values of R^2 (>0.93). Here it is also shown that the accumulated volume as a function of time follows the same type of ODE. The values of n between the four original discreate values could be physically interpreted as the existence of new blocking mechanisms.

Keywords: Membrane fouling, Hermia model, Fouling model, Pore blocking, Blocking mechanism.

1. Introduction

One of the most widely used models to predict membrane fouling is the Hermia model [1]. In the 1982 paper, Hermia was able to frame mathematically the relationship between the accumulated volume and time from experimental data, arriving at the differential equation presented in Section 2.3. Since this model was derived for non-newtonian fluids, the parameters n and k help to adjust the model for different types of fluids and blocking mechanisms. The original ordinary differential equation (ODE) was solved for four different discrete values of n, each value with its own blocking mechanism, as shown in Figure 1 and in Equations 1-4.

Where t is the time measured from the beginning of the filtration experiment, j is the permeate flux at time t, j_0 is the permeate flux at time $t = 0$ and k is a real constant determined experimentally. The simplicity and effectiveness of this model made its way into the application of membrane filtration, such as the ultrafiltration of polyethylene glycol [2], cross flow ultrafiltration of waste water [3], nanofiltration of polycyclic aromatic hydrocarbons [4], particle fouling during microfiltration [5] and natural organic matter fouling [6]. Although the Hermia model works well for the original four values of n, there are applications where the permeate flux is discontinuous, such as the removal of glycerol from biodiesel [7,8] or in high-pressure nanofiltration [9], in which these values cannot accommodate experimental data.

 doi:10.20944/preprints202206.0187.v1

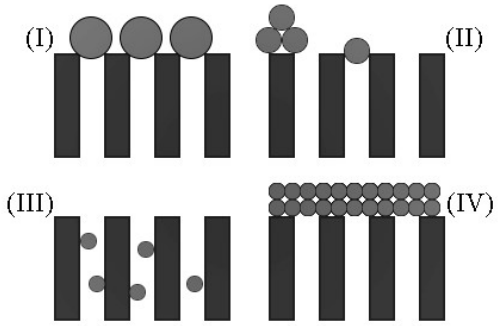

Figure 1. Blocking mechanisms by Hermia (1982): (I) complete blocking; (II) intermediate blocking; (III) standard blocking; (IV) cake formation.

Complete blocking ($n = 2$)	$\ln j = \ln j_0 - k \cdot t$	(1)
Intermediate blocking ($n = 1$)	$1/j = (1/j_0) - k \cdot t$	(2)
Standard blocking ($n = 3/2$)	$1/\sqrt{j} = (1/\sqrt{j_0}) - k \cdot t$	(3)
Cake formation ($n = 0$)	$1/j^2 = (1/j_0^2) - k \cdot t$	(4)

Therefore, this model has been modified to better accommodate experimental results by increasing its complexity, either by keeping the same blocking mechanisms but changing the equations, such as in glycerin-water solutions [10], or by using the concept of flow resistance, as in oil-water emulsions [11], still both these modifications use the original Hermia model as the base. Similar approaches have been used to model fouling in micro- and ultrafiltration membranes for treating limed and partially clarified sugar cane juice [12], such as the use of pore narrowing models and the combination of external and progressive internal fouling.

Since Equations 1-4 were obtained only for four discrete values of n, the original model is limited to these values. Therefore, this work aims not only to prove the original Hermia model from the experimental ODE, but also to broaden its use by proving a general solution for any real number n through the equations of fluid mechanics and the properties of single and multivariable calculus.

2. Materials and Methods

2.1. Control Volume and Model Setup

Inside of a module (Figure 2) of constant cross-sectional area A with a constant mass flux N_0, some mass from this flux will be retained by the membrane making it harder for more mass to pass through the membrane as permeate. As a consequence, over time, the exit mass flux $N(t)$ should decrease. In this model, the mass accumulated is modeled by a porous solid with a constant base area A and thickness $\delta(t)$. After an infinitesimal time Δt, the mass accumulated makes δ to increase. Therefore, it is possible to take this solid as the control volume (CV) and apply conservation laws to it.

Preprints (www.preprints.org) | NOT PEER-REVIEWED | Posted: 13 June 2022 doi:10.20944/preprints202206.0187.v1

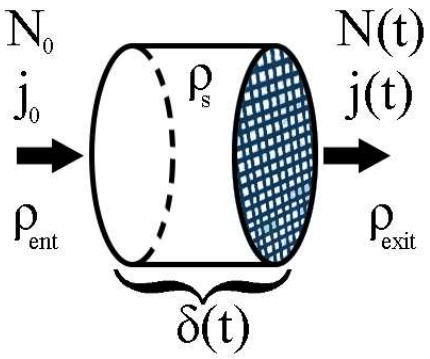

Figure 2. The control volume is a solid with a constant cross-sectional area A and density ρ_s, such that the entering stream of fluid has a constant mass flux N_0, a constant permeate flux j_0 and density ρ_{ent}. The exiting stream of fluid has a mass flux $N(t)$, a permeate flux $j(t)$ and density ρ_{exit}. The length $\delta(t)$ increases over time as more mass is accumulated on the membrane (shown as shaded section).

2.2. Continuity Equation

The continuity equation (Eq. 5), also known as the general conservation of mass equation [13] or as the mass balance equation [14], is the mathematical formula that keeps track of how much mass is inside of a given control volume. It does so by computing how much the control volume itself changes over time, which is given by the volume integral, and by calculating how much mass leaves or enters the CV, which is given by the surface integral.

$$\frac{\partial}{\partial t}\iiint_{CV} \rho d\forall + \iint_{CS} \rho(\vec{j}\cdot\vec{n})dA = 0 \quad (5)$$

Where ρ is the density function, $d\forall$ is the volume differential of the CV, $\vec{j}$ is the velocity vector, $\vec{n}$ is the vector perpendicular to the surface of the CV and dA is the differential surface area of the CV.

2.3. Hermia's Experimental Model

The differential equation (Eq. 6) is an experimental result obtained by Hermia [1], which correlates the second derivative of time (t) with respect to the accumulated volume (V) with the first derivative of t with respect to V.

$$\frac{d^2t}{dV^2} = k\left(\frac{dt}{dV}\right)^n \quad (6)$$

Here, the coefficients k and n are two real numbers that can be changed to better adjust the model for different situations. As discussed in Section 1, the model was originally solved for $n = 2, 1{,}3/2, 0$. These solutions resulted in Equations 1-4, respectively.

2.4. Derivatives of Inverse Functions

For a given function $y(x)$ and its inverse function given by $x(y)$, the relationship between dy/dx and dx/dy, if $y(a) = b$, is given by [15]:

$$\left(\frac{dy}{dx}\right)_{x=a}\cdot\left(\frac{dx}{dy}\right)_{y=b} = 1 \quad (7)$$

As for the second derivatives of these functions:

$$\left(\frac{d^2y}{dx^2}\right)_{x=a} = -\left(\frac{d^2x}{dy^2}\right)_{y=b}\cdot\left[\left(\frac{dy}{dx}\right)_{x=a}\right]^3 \quad (8)$$

Preprints (www.preprints.org) | NOT PEER-REVIEWED | Posted: 13 June 2022 doi:10.20944/preprints202206.0187.v1

For the sake of brevity, the proof does not use the full subscript (e.g., $x = a$). It only discloses the direct values of the independent variables. As an example, $(dy/dx)_{x=a}$ would be written as $(dy/dx)_a$

2.5. Flux Definition

One of the definitions of mass flux of a given stream i is given by the product between its mass concentration/total density (ρ_i) and its velocity (j_i) [13, 14], as stated in Equation 9.

$$N_i = \rho_i j_i \tag{9}$$

2.6. Accumulated Volume and Flux

As presented in Equation 10, the accumulated volume $V(t)$ for a mass flux $N(t)$ can be calculated by integrating $N(t)$ from t = 0 to t = t, which will give the total mass per unit of cross-sectional area. Therefore, multiplying by the area and dividing by its density will yield the accumulated volume, $V(t)$.

$$V(t) = \frac{A}{\rho_{exit}} \int_0^t N(t)dt \tag{10}$$

2.7. Integral Properties

A reduced form of the Leibnitz formula with constant integration limits a and b for a given function $y(x)$ yields Equation 11 [16].

$$\int_a^b \left[\frac{dy(x)}{dx}\right] dx = y(b) - y(a) \tag{11}$$

3. Results

3.1. Model Proof

Taking all of the equations presented in Section 2, it is possible to take the control volume from Section 2.1 and apply the continuity equation (Section 2.2). By making the assumption that the system has uniform entrances and exits, the surface integral can be reduced to:

$$\iint_{CS} \rho\vec{j} \cdot d\vec{A} = \sum_{CS} \rho_i j_i A_i \tag{12}$$

For the present system, there are two sources of flux, the entrance and the exit. As a result, this sum is given by:

$$\sum_{CS} \rho_i j_i A_i = \rho_{exit} j(t) A_{exit} - \rho_{ent} j_0 A_{ent} \tag{13}$$

By the definition of flux given on Section 2.5, $N_0 = \rho_{in} j_0$ and $N(t) = \rho_{out} j(t)$. Since the control volume has a constant area, $A_{exit} = A_{ent} = A$. Therefore:

$$\sum_{CS} \rho_i j_i A_i = A \cdot (N(t) - N_0) \tag{14}$$

Thus, the surface integral of the Continuity Equation is simplified to:

$$\iint_{CS} \rho\vec{j} \cdot d\vec{A} = A \cdot (N(t) - N_0) \tag{15}$$

Preprints (www.preprints.org) | NOT PEER-REVIEWED | Posted: 13 June 2022 doi:10.20944/preprints202206.0187.v1

As for the volume integral, since the control volume itself is a porous solid with a constant density ρ_s, a base area A and length $\delta(t)$:

$$\iiint_{CV} \rho d\forall = \rho_s \forall = \rho_s \cdot A \cdot \delta(t) \tag{16}$$

So:

$$\frac{\partial}{\partial t} \iiint_{CV} \rho d\forall = \rho_s \cdot A \cdot \frac{d\delta(t)}{dt} \tag{17}$$

Going back to the Continuity Equation:

$$\rho_s \cdot A \cdot \frac{d\delta(t)}{dt} + A \cdot (N(t) - N_0) = 0$$

If $k_1 = \rho_s$, then:

$$N(t) = N_0 - k_1 \cdot \frac{d\delta(t)}{dt} \tag{18}$$

According to [1], for a real constant k_2:

$$\frac{d^2t}{dV^2} = k_2 \left(\frac{dt}{dV}\right)^n \tag{19}$$

Using the first property presented on Section 2.4, it is possible to write dt/dV in terms of dV/dt. Therefore:

$$\left(\frac{dt}{dV}\right)_{V^*} = \left[\left(\frac{dV}{dt}\right)_{t^*}\right]^{-1} \tag{20}$$

For $V(t^*) = V^*$. Now using the second property from the same Section, it is possible to write d^2t/dV^2 in terms of dV^2/dt^2. Thus, Eq. 19 can be rewritten as:

$$\left(\frac{d^2t}{dV^2}\right)_{V^*} = -\left(\frac{d^2V}{dt^2}\right)_{t^*} \cdot \left[\left(\frac{dt}{dV}\right)_{V^*}\right]^3$$

Using Eq. 20:

$$\left(\frac{d^2t}{dV^2}\right)_{V^*} = -\left(\frac{d^2V}{dt^2}\right)_{t^*} \cdot \left[\left(\frac{dV}{dt}\right)_{t^*}\right]^{-3} \tag{21}$$

Applying Eq. 20 and 21 into the Hermia model:

$$\left[-\left(\frac{d^2V}{dt^2}\right)_{t^*} \cdot \left[\left(\frac{dV}{dt}\right)_{t^*}\right]^{-3}\right] = k_2 \cdot \left\{\left[\left(\frac{dV}{dt}\right)_{t^*}\right]^{-1}\right\}^n$$

$$\left(\frac{d^2V}{dt^2}\right)_{t^*} = k_3 \left[\left(\frac{dV}{dt}\right)_{t^*}\right]^{3-n}$$

If $m = 3 - n$ and k_3 is another real constant, then:

$$\left(\frac{d^2V}{dt^2}\right)_{t^*} = k_3 \left[\left(\frac{dV}{dt}\right)_{t^*}\right]^m$$

Since both of these derivatives have the same domain of t, then for any t^*, this ODE is valid, therefore it is possible to remove the subscript.

$$\frac{d^2V}{dt^2} = k_3 \left[\left(\frac{dV}{dt}\right)\right]^m \tag{22}$$

It is important to note that both Equations 6 and 22 are analogous, which means that both functions $t(V)$ and $V(t)$ are solutions of the same family of differential equations. By the definition of accumulated volume presented in Section 2.6, it is possible to use the Equation 18, such that;

Preprints (www.preprints.org) | NOT PEER-REVIEWED | Posted: 13 June 2022 doi:10.20944/preprints202206.0187.v1

$$V(t) = \frac{A}{\rho_{exit}} \int_0^t \left[N_0 - k_1 \frac{d\delta(t)}{dt} \right] dt$$

By the integral property presented in Section 2.6:

$$\int_0^t \left[\frac{d\delta(t)}{dt} \right] dt = \delta(t) - \delta(0)$$

Since there is no mass accumulated in the control volume at $t = 0$, then $\delta(0) = 0$. As a result:

$$V(t) = \frac{A}{\rho_{exit}} [N_0 \cdot t - k_1 \delta(t)] \quad (23)$$

Differentiating $V(t)$ twice:

$$\frac{dV}{dt} = \frac{A}{\rho_{exit}} \left[N_0 - k_1 \frac{d\delta(t)}{dt} \right] \quad (24)$$

$$\frac{d^2V}{dt^2} = -k_1 \frac{A}{\rho_{exit}} \cdot \frac{d^2\delta(t)}{dt^2} \quad (25)$$

With these derivatives, it is possible to rewrite Equation 22, such that:

$$-k_1 \frac{A}{\rho_l} \cdot \frac{d^2\delta(t)}{dt^2} = k_3 \left[\frac{A}{\rho_{exit}} \left[N_0 - k_1 \frac{d\delta(t)}{dt} \right] \right]^m$$

For another real constant k_4:

$$\frac{d^2\delta(t)}{dt^2} = k_4 \left[N_0 - k_1 \frac{d\delta(t)}{dt} \right]^m \quad (26)$$

Reducing Eq. 26 further with Eq. 18:

$$\frac{d^2\delta(t)}{dt^2} = k_4 [N(t)]^m \quad (27)$$

By differentiating Eq. 18:

$$\frac{dN(t)}{dt} = -k_1 \frac{d^2\delta(t)}{dt^2} \quad (28)$$

Therefore, Eq. 27 can be simplified further to:

$$\frac{dN(t)}{dt} = k_5 [N(t)]^m \quad (29)$$

Such that k_5 is another real constant. Now, by applying the separation of variables method [17]:

$$[N(t)]^{-m} dN(t) = k_5 dt$$

As a result, for $m \neq 1$:

$$\int_{N(0)}^{N(t)} [N(t)]^{-m} dN(t) = \int_0^t k_5 dt$$

$$\left[\frac{[N(t)]^{(1-m)}}{(1-m)} \right]_{N(0)}^{N(t)} = [k_5 t]_0^t$$

$$\frac{1}{(1-m)} \{ [N(t)]^{1-m} - [N(0)]^{1-m} \} = k_5 t$$

$$[N(t)]^{1-m} = [N(0)]^{1-m} + (1-m) k_5 t$$

If $P = 1 - m$:

$$[N(t)]^P = [N(0)]^P + P \cdot k_5 \cdot t$$

And $Pk_5 = -k_6$:

$$[N(t)]^P = [N(0)]^P - k_6 \cdot t$$

 doi:10.20944/preprints202206.0187.v1

Since there is no mass accumulated at the beginning of the filtration experiment ($\delta(0) = 0$), both N_0 and $N(0)$ are equal. Therefore:

$$[N(t)]^P = [N_0]^P - k_6 \cdot t \qquad (30)$$

It is important to notice that Eq. 30 is similar to the original equations used in the Hermia model. It is also important to highlight that both P and k_6 can assume any real values, as long as $P \neq 0$. By using the flux definition presented in Section 2.4

$$[\rho_{exit} j(t)]^P = [\rho_{ent} j_0]^P - k_6 \cdot t$$

Thus, if k_7 is another real constant:

$$[j(t)]^P = \left[\frac{\rho_{ent}}{\rho_{exit}}\right]^P \cdot j_0^P - k_7 \cdot t \qquad (31)$$

As a result, Eq. 31 closely resembles the power law used in the Hermia fouling model. However, the additional term $[\rho_{ent}/\rho_{exit}]^P$ correctly scales up j_0 such that the right-hand side of Eq. 31 agrees with the Continuity Equation. In special cases where the density of the permeate is close to the original density ($\rho_{exit} \to \rho_{ent}$), the correction term $[\rho_{ent}/\rho_{exit}]^P \to 1$. If that is the case, $[j(t)]^P$ can be approximated by:

$$[j(t)]^P \approx j_0^P - k_7 \cdot t \qquad (32)$$

Taking a closer look into Eq. 31 and 32, it is interesting to point out that as $P \to \infty$, all terms with the exponent P become larger than $k_7 \cdot t$. Hence in both cases $j(t)$ will end up as a constant value. For the special case when $m = 1$:

$$\int_{N_0}^{N(t)} \frac{1}{N(t)} dN(t) = \int_0^t k_5 dt$$

$$\ln\left[\frac{N(t)}{N_0}\right] = k_5 t$$

$$N(t) = N_0 \exp(k_5 t)$$

If $k_9 = -k_5$, then:

$$N(t) = N_0 \exp(-k_9 t) \qquad (33)$$

Since Equation 33 has an exponential function multiplying N_0, and k_9 can assume positive values (or $k_5 < 0$), when $m = 1$, the system can behave with a classical drop for $N(t)$. Applying again the flux definition presented in Section 2.5:

$$\rho_{exit} j(t) = \rho_{ent} j_0 \, exp(-k_9 t)$$

$$j(t) = j_0 \left[\frac{\rho_{ent}}{\rho_{exit}}\right] exp(-k_9 t) \qquad (34)$$

For the same reasons as before, if $\rho_{exit} \to \rho_{ent}$, $[\rho_{ent}/\rho_{exit}] \to 1$ and $j(t)$ can be approximated by:

$$j(t) \approx j_0 \, exp(-k_9 t) \qquad (35)$$

Since $m = 3 - n$ and $P = 1 - m$, it is possible to conclude that $P = 2 - n$. By using the four original discreate values of $n = 2, 1, 3/2, 0$, $P = 0, -1, -1/2, -2$, which are exactly the respective exponents of j in Eq. 1-4. Thus, through Eq. 32 and 35, it is possible to reproduce the entire Hermia model. Since Eq. 32 was obtained for any real n different than 2 and Eq. 35 was obtained for $n = 2$, these equations form a model that can be used for any real n, which widens the usefulness of the Hermia model considerably. Consequently, there are also values of n between the four original discrete values, which can be physically interpreted as the existence of new types of fouling mechanisms in membranes. Using Eq. 18, 31 and 34, it is possible to deduce how the fouling profile should

 doi:10.20944/preprints202206.0187.v1

change with P, given by the function $\delta(t)$. Through Eq. 9 and 18, it is possible to show that:

$$\left[\frac{j(t)}{j_0}\right] = \left[\frac{\rho_{ent}}{\rho_{exit}}\right] - k_{10}\frac{d\delta(t)}{dt} \qquad (36)$$

For another real constant k_{10}. For the case of $P \neq 0$, the profile of $j(t)$ is given by Eq. 31. Taking this equation and dividing both sides by j_0^P:

$$\left[\frac{j(t)}{j_0}\right]^P = \left[\frac{\rho_{ent}}{\rho_{exit}}\right]^P - k_7 t \qquad (37)$$

Since k_7/j_0^P is still a constant in Eq. 37, the same constant will be used. Therefore, by substituting Eq. 36 into Eq. 37:

$$\left[\left[\frac{\rho_{ent}}{\rho_{exit}}\right] - k_{10}\frac{d\delta(t)}{dt}\right]^P = \left[\frac{\rho_{ent}}{\rho_{exit}}\right]^P - k_7 t$$

$$\left[\frac{\rho_{ent}}{\rho_{exit}}\right] - k_{10}\frac{d\delta(t)}{dt} = \left(\left[\frac{\rho_{ent}}{\rho_{exit}}\right]^P - k_7 t\right)^{1/P}$$

$$-k_{10}\frac{d\delta(t)}{dt} = \left(\left[\frac{\rho_{ent}}{\rho_{exit}}\right]^P - k_7 t\right)^{\frac{1}{P}} - \left[\frac{\rho_{ent}}{\rho_{exit}}\right]$$

If k_{11} and k_{12} are other real constants, then:

$$\frac{d\delta(t)}{dt} = k_{11}\left(\left[\frac{\rho_{ent}}{\rho_{exit}}\right]^P - k_7 t\right)^{\frac{1}{P}} + k_{12}$$

$$\frac{d\delta(t)}{dt} = \left(k_{11}^P\left[\frac{\rho_{ent}}{\rho_{exit}}\right]^P - k_{11}^P k_7 t\right)^{\frac{1}{P}} + k_{12}$$

Thus, if $k_{13} = k_{11}^P[\rho_{ent}/\rho_{exit}]^P$ and $k_{14} = -k_{11}^P k_7$:

$$\frac{d\delta(t)}{dt} = (k_{13} + k_{14}t)^{\frac{1}{P}} + k_{12} \qquad \textbf{(38)}$$

Now, by applying the separation of variables method in Eq. 38 [17]:

$$\int_{\delta(0)}^{\delta(t)} d\delta(t) = \int_0^t [(k_{13} + k_{14}t)^{\frac{1}{P}} + k_{12}]dt$$

Since:

$$\int_{\delta(0)}^{\delta(t)} d\delta(t) = \delta(t) - \delta(0)$$

And $\delta(0) = 0$, then:

$$\delta(t) = \int_0^t [(k_{13} + k_{14}t)^{\frac{1}{P}} + k_{12}]dt \qquad (39)$$

By integrating Eq. 39 with respect to t:

$$\delta(t) = \left[\frac{1}{k_{14}}\frac{(k_{13} + k_{14}t)^{\frac{1}{P}+1}}{\left(\frac{1}{P}+1\right)} + k_{12}t\right]_0^t$$

$$\delta(t) = \frac{1}{k_{14}}\left[\frac{(k_{13} + k_{14}t)^{\frac{1}{P}+1} - k_{13}^{\frac{1}{P}+1}}{\left(\frac{1}{P}+1\right)}\right] + k_{12}t$$

Preprints (www.preprints.org) | NOT PEER-REVIEWED | Posted: 13 June 2022 doi:10.20944/preprints202206.0187.v1

It is possible to further reduce this equation by distributing the terms $1/k_{14}$ and $(1/P+1)$. By doing that, it should be possible to regroup the constants inside the brackets of $(k_{13}+k_{14}t)^{\frac{1}{P}+1}$. If:

$$k_{15}=\frac{k_{13}}{\left(k_{14}\cdot\left(\frac{1}{P}+1\right)\right)^{\frac{P}{P+1}}}$$

$$k_{16}=\frac{k_{14}}{\left(k_{14}\cdot\left(\frac{1}{P}+1\right)\right)^{\frac{P}{P+1}}}$$

$$k_{17}=\frac{-k_{13}^{\frac{1}{P}+1}}{k_{14}\cdot\left(\frac{1}{P}+1\right)}$$

Then:

$$\delta(t)=(k_{15}+k_{16}t)^{\frac{1}{P}+1}+k_{17}+k_{12}t \qquad (40)$$

By applying $\delta(0)=0$ in Eq. 40, it can be found that:

$$k_{17}=-k_{15}^{\frac{1}{P}+1}$$

As a result, Eq. 40 can be further reduced to:

$$\delta(t)=(k_{15}+k_{16}t)^{\frac{1}{P}+1}-k_{15}^{\frac{1}{P}+1}+k_{12}t \qquad (41)$$

For the case of $P=0$, through Eq. 34 and 36, it is possible to show that:

$$\left[\frac{\rho_{ent}}{\rho_{exit}}\right]exp(-k_9t)=\left[\frac{\rho_{ent}}{\rho_{exit}}\right]-k_{10}\frac{d\delta(t)}{dt}$$

Dividing both sides by $[\rho_{ent}/\rho_{exit}]$:

$$exp(-k_9t)=1-k_{10}\left[\frac{\rho_{exit}}{\rho_{ent}}\right]\frac{d\delta(t)}{dt}$$

If $1/k_{18}=-k_{10}[\rho_{exit}/\rho_{ent}]$, then:

$$exp(-k_9t)=1+\frac{1}{k_{18}}\frac{d\delta(t)}{dt}$$

Therefore:

$$\frac{d\delta(t)}{dt}=k_{18}[exp(-k_9t)-1] \qquad (42)$$

Now, by applying the separation of variables method in Eq. 42 [16]

$$\int_{\delta(0)}^{\delta(t)}d\delta(t)=k_{18}\int_0^t[exp(-k_9t)-1]\,dt$$

$$\delta(t)=k_{18}\left[\frac{1}{-k_9}exp(-k_9t)-t\right]_0^t$$

$$\delta(t)=-\frac{k_{18}}{k_9}[exp(-k_9t)-1]-k_{18}t$$

If $k_{19}=-k_{18}/k_9$ and $k_{20}=-k_{18}$, then:

$$\delta(t)=k_{19}[exp(-k_9t)-1]+k_{20}t \qquad (43)$$

 doi:10.20944/preprints202206.0187.v1

As a result, with Eq. 41 and 43, it is possible to construct a fouling model for every real value of P, such that:

$$\delta(t) = \begin{cases} (k_{15} + k_{16}t)^{\frac{1}{P}+1} - k_{15}^{\frac{1}{P}+1} + k_{12}t, P \neq 0 \\ k_{19}[\exp(-k_9 t) - 1] + k_{20}t, P = 0 \end{cases} \quad (44)$$

It is important to notice that the different fouling profiles δ are given by the exponent $1/P + 1$. Therefore, by analyzing this exponent, it is possible to draw conclusions about the fouling profiles as well. By taking the limit as $P \to \infty$, $1/P \to 0$:

$$\delta(t) = (k_{15} + k_{16}t)^{0+1} - k_{15}^{0+1} + k_{12}t$$

$$\delta(t) = (k_{16} + k_{12})t$$

Now, by taking the limit as $P \to -\infty$, $1/P \to 0$:

$$\delta(,t) = (k_{15} + k_{16}t)^{0+1} - k_{15}^{0+1} + k_{12}t$$

$$\delta(t) = (k_{16} + k_{12})t$$

Therefore, for both $P \to \infty$ and $P \to -\infty$, the result is a linear curve. The same behavior can be seen when $P = -1$, since:

$$\delta(t) = (k_{15} + k_{16}t)^{1-1} - k_{15}^{1-1} + k_{12}t$$

$$\delta(t) = k_{12}t$$

For positive values of P, the exponent $1/P + 1$ is always larger than 1, in contrast for negative values of P, $1/P + 1$ is always smaller than 1. Consequently, there is one and only one unique fouling profile $\delta(t)$ for every real value P.

3.2. Application of the Generalized Hermia Model

To better illustrate how the Generalized Hermia model can be used, this model has been fitted to already published data ([17], [18], [19], [20], [21], [22], [23]). The model fitting was done in terms of the specific membrane flux, given by j/j_0. Assuming that both the entrance and exit densities are approximately the same, it is possible to use Equation 32, such that:

$$\left[\frac{j(t)}{j_0}\right]^P \approx 1 - \frac{k_7}{j_0^P} \cdot t$$

If k_7/j_0^P is another real constant k, then:

$$\left[\frac{j(t)}{j_0}\right]^P \approx 1 - k \cdot t \quad (45)$$

Thus, by using Equation 45, the values presented in Tables 1-7.

3.2.1. Applications in Ultrafiltration

From the fitting data presented in Table 1 and in Figures 3, 4 and 5, it is possible to point out that different filtration conditions, such as different cross flow rates (CFRs) and different trans-membrane pressures (TMPs) amount to different coefficients k and P. Based on the data used for the model fitting, if CFR in maintained constant, an increase in TMP does not seem to cause any significant changes to either k or P, apart from the last fit presented in Table 1. On the contrary, by keeping the TMP constant, an increase in CFR amounts to a slight increase in k, which implies that, in the present case, $j(t)$ decreases more rapidly as a result. An increase on CFR while keeping the TMP constant does not seem to affect P.

 doi:10.20944/preprints202206.0187.v1

Table 1. Model fitting for different filtration conditions in oily effluent treatment [17]

Filtration mechanism	CFR (L/h)	TMP (kPa)	k (min^{-1})	P
Ultrafiltration	14	21	-0.38355	-1.565
Ultrafiltration	14	35	-0.37436	-1.494
Ultrafiltration	14	104	-0.37012	-1.468
Ultrafiltration	28	21	-0.36630	-1.428
Ultrafiltration	28	35	-0.38615	-1.498
Ultrafiltration	28	104	-0.38687	-1.488
Ultrafiltration	40	21	-0.39749	-1.515
Ultrafiltration	40	35	-0.39230	-1.499
Ultrafiltration	40	104	-0.4489	-1.578

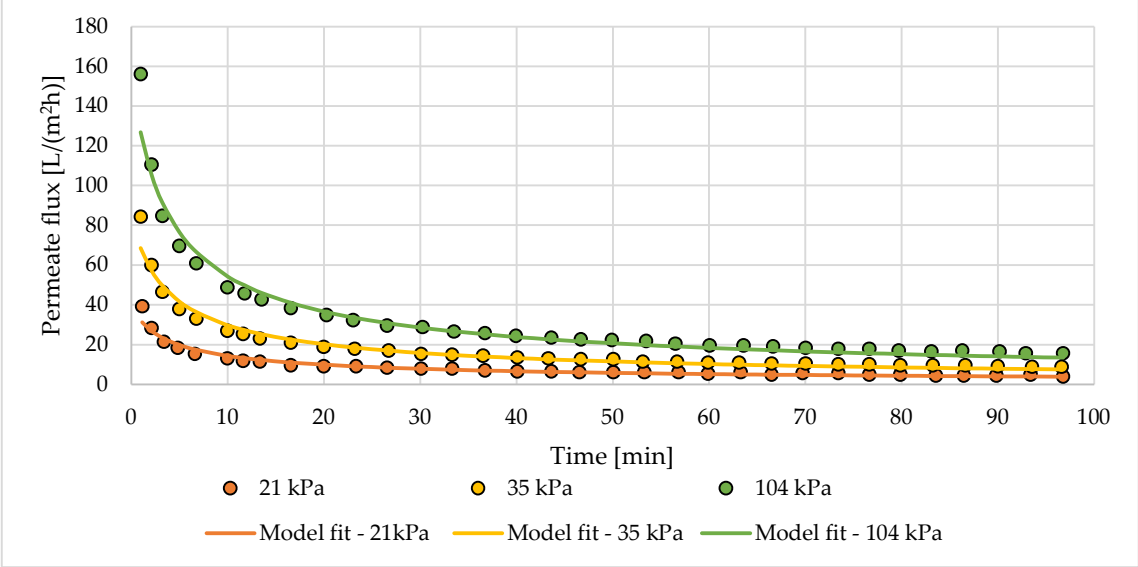

Figure 3. Model fitting for different filtration conditions in oily effluent treatment at CFR of 14 L/h [17].

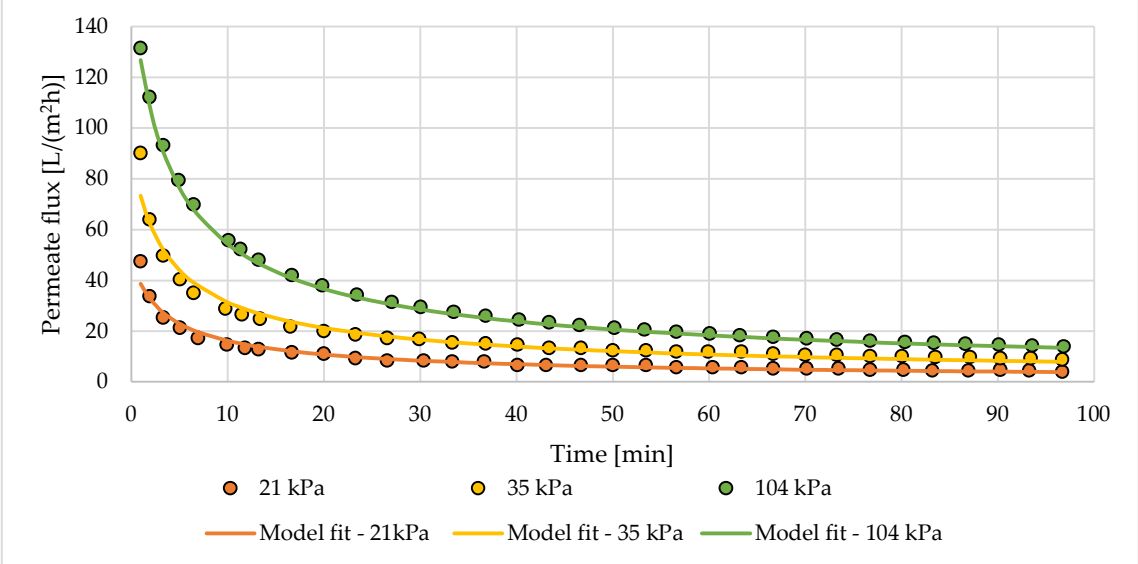

Figure 4. Model fitting for different filtration conditions in oily effluent treatment at CFR of 28 L/h [17].

Preprints (www.preprints.org) | NOT PEER-REVIEWED | Posted: 13 June 2022 doi:10.20944/preprints202206.0187.v1

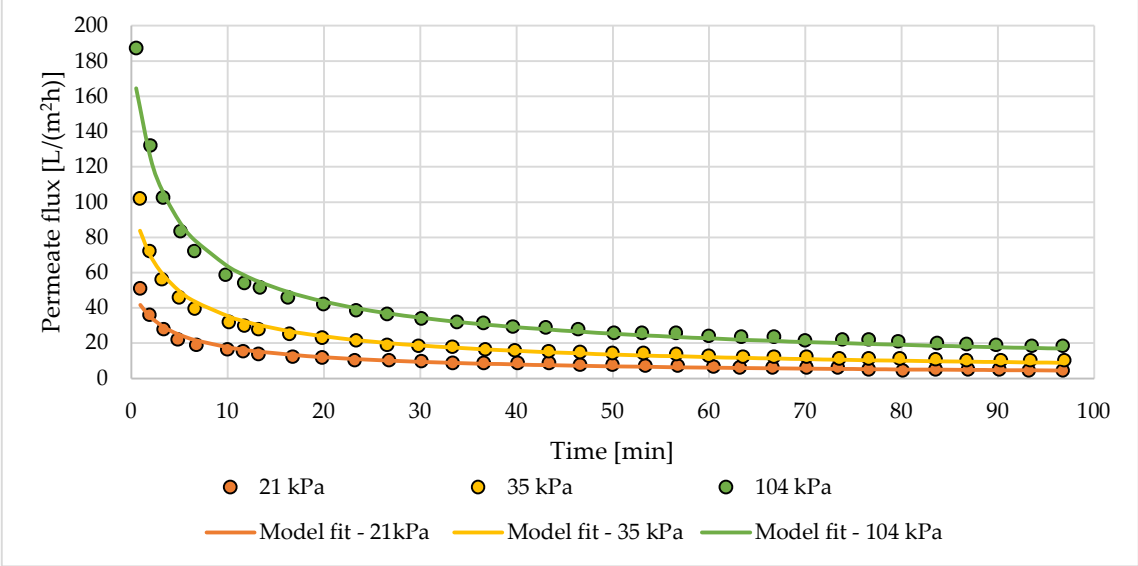

Figure 5. Model fitting for different filtration conditions in oily effluent treatment at CFR of 40 L/h [17].

As for the model fitting presented in Table 2 and in Figures 6 and 7, it is clear that different membrane types influence the coefficients, given the considerable gap between the both k and P when comparing membranes with hydrophilic (HPI) matter against membranes with hydrophobic (HPO) matter. According to the data used, the application of coagulating agents (Coag.) and of additives such as MIEX® also influence the coefficients, since both cause a sharp decline in k on all tests presented in Table 2. In both HPI and HPO membranes, the addition of the coagulating agent caused an increase in P, while the opposite happened with the addition of MIEX®.

Table 2. Model fitting for different filtration conditions in desalination and water treatment [18]

Filtration mechanism	Experimental Conditions	k (h^{-1})	P	R^2
Ultrafiltration	HPI UF only	-11.69	-2.855	0.9989
Ultrafiltration	Coag. 140mg/L+HPI UF	-9.558	-4.432	0.9959
Ultrafiltration	MIEX 12mL/L+UF	-9.328	-2.882	0.9984
Ultrafiltration	MIEX 12mL/L+Coag. 40mg/L+HPI UF	-2.407	-3.084	0.9971
Ultrafiltration	HPO UF	-99.2	-2.228	0.995
Ultrafiltration	Coag. 140mg/L+HPO UF	-26.12	-3.063	0.9964
Ultrafiltration	MIEX 12mL/L+HPO UF	-25.94	-1.845	0.9978
Ultrafiltration	MIEX 12mL/L+Coag. 40mg/L+HPO UF	-17.49	-2.965	0.9964

 doi:10.20944/preprints202206.0187.v1

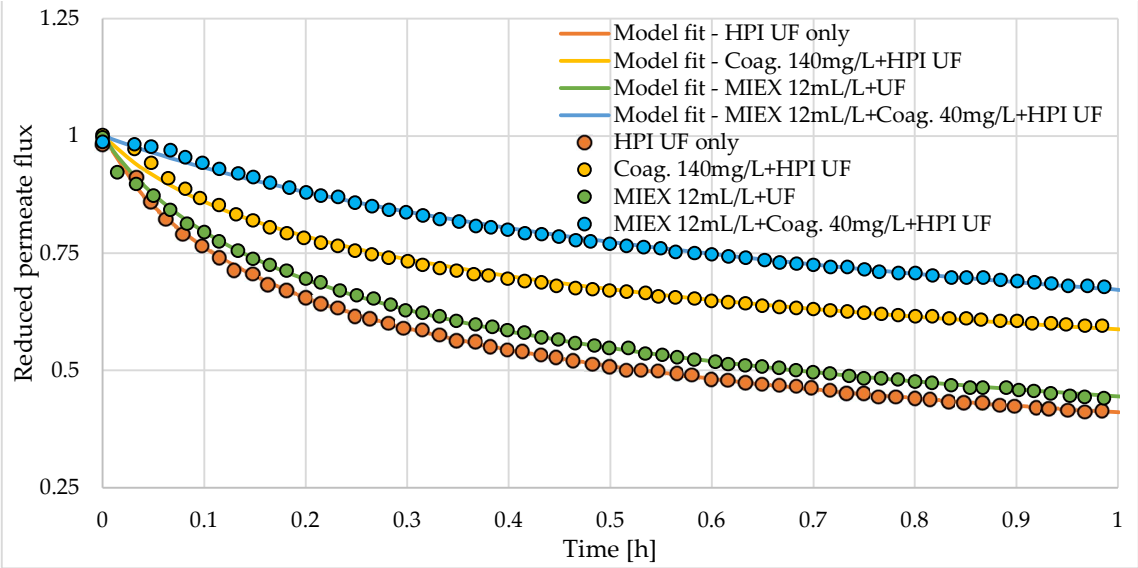

Figure 6. Model fitting for different hydrophilic filtration conditions in desalination and water treatment [18]

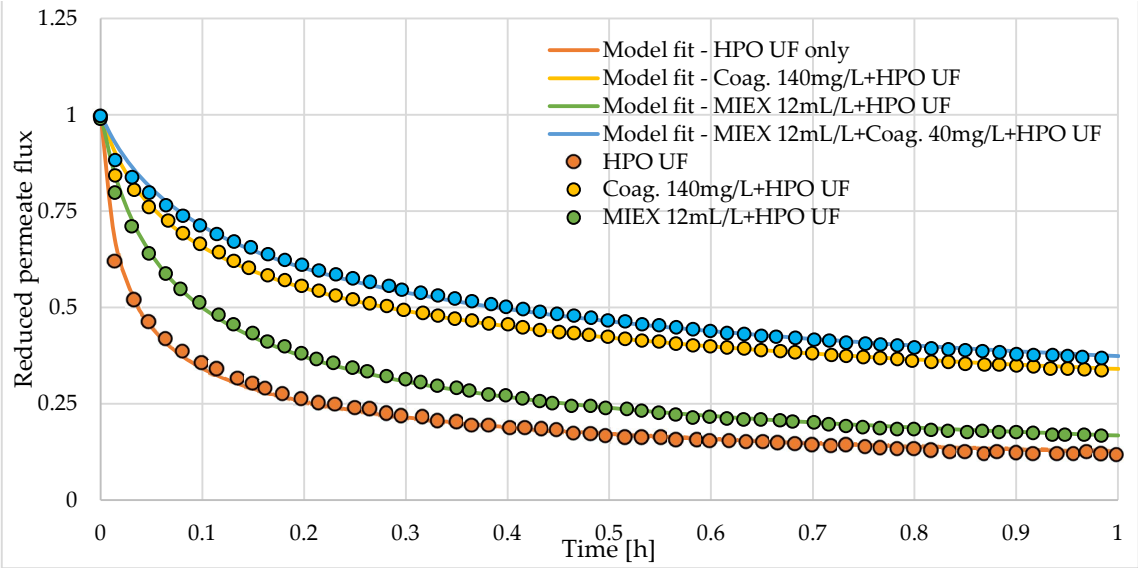

Figure 7. Model fitting for different hydrophobic filtration conditions in desalination and water treatment [18]

The fitting presented in Table 3 and in Figures 8 and 9 indicates how fouling accumulates over many cycles of operation. The original work proposed in [19] aimed to reduce fouling by coating the membrane PolySBMA. As shown in Table 3, both coated and uncoated membranes showed an increase in k on later cycles, as well as different values of P. This increase in k indicates that $j(t)$ decreases more rapidly in later cycles. It is also evident that coating the membrane is advantageous since k is much smaller in later cycles.

Preprints (www.preprints.org) | NOT PEER-REVIEWED | Posted: 13 June 2022 doi:10.20944/preprints202206.0187.v1

Table 3. Model fitting for different filtration conditions of bovine serum albumin solutions [19]

Filtration mechanism	Coated or Uncoated	Cycles	k (h^{-1})	P	R^2
Ultrafiltration	Uncoated	1st	-5.580	-1.536	0.9866
Ultrafiltration	Uncoated	2nd	-25.850	-1.878	0.9947
Ultrafiltration	Uncoated	3rd	-38825	-4.921	0.9889
Ultrafiltration	Coated	1st	-4.189	-1.715	0.9882
Ultrafiltration	Coated	2nd	-35.017	-2.474	0.9332
Ultrafiltration	Coated	3rd	-102.485	-4.205	0.9782

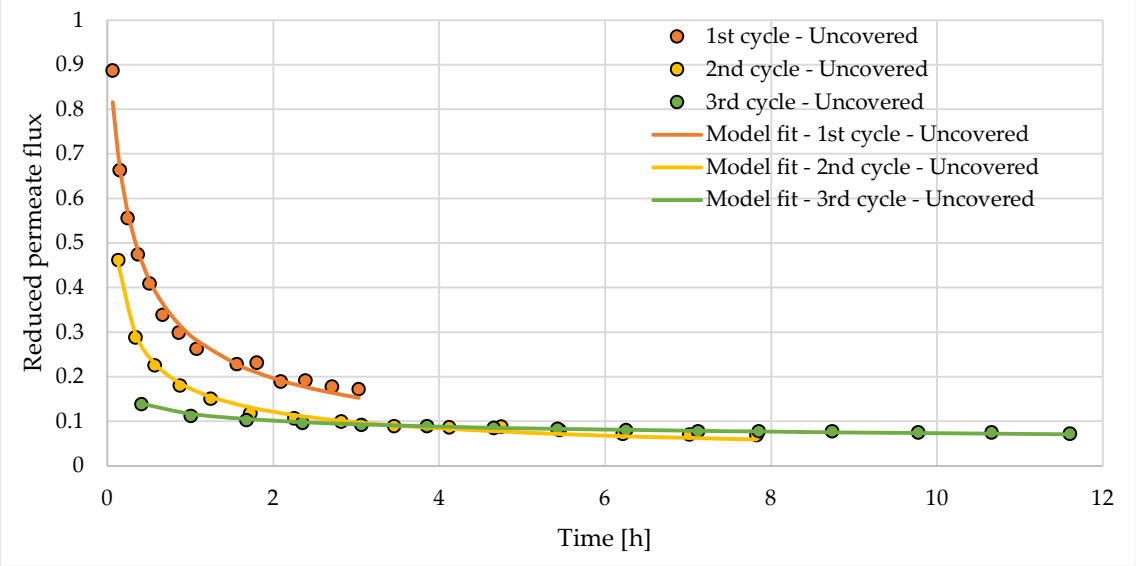

Figure 8. Model fitting for filtration conditions of bovine serum albumin solutions in uncoated membranes [19]

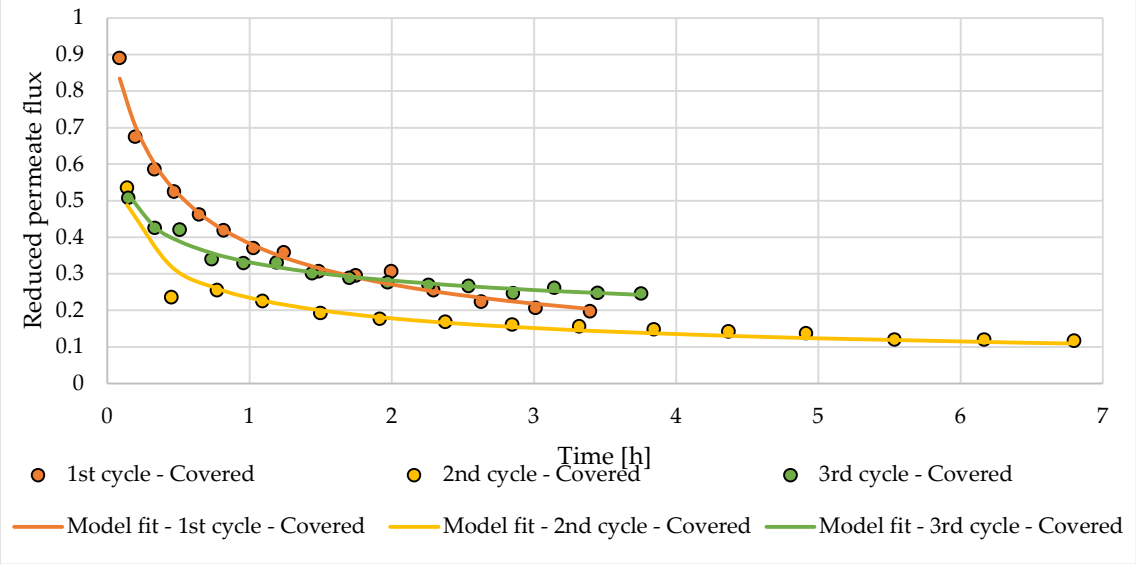

Figure 9. Model fitting for filtration conditions of bovine serum albumin solutions in coated membranes [19]

 doi:10.20944/preprints202206.0187.v1

As for the fitting data presented in Table 4 and in Figures 10 and 11, the influence of the TMP and the concentration of nanoparticles (NPs) (given in mg of nanoparticles per liter or mg NPs/L) are evaluated. For both TMPs presented in Table 4, the increase in concentration of nanoparticles caused an increase in k, while P has both increased and decreased with nanoparticle concentration.

Table 4. Model fitting for different filtration conditions of nanoparticles in polishing wastewater [20]

Filtration mechanism	mg NPs/L	TMP (bar)	k (s^{-1})	P	R^2
Ultrafiltration	97	0.4	-0.02613	-3.602	0.9866
Ultrafiltration	251	0.4	-0.01384	-2.064	0.9947
Ultrafiltration	657	0.4	-0.18643	-2.797	0.9889
Ultrafiltration	332	0.3	-0.06550	-7.686	0.9882
Ultrafiltration	572	0.3	-4.55004	-12.37	0.9332
Ultrafiltration	2600	0.3	-7.88155	-9.01	0.9782

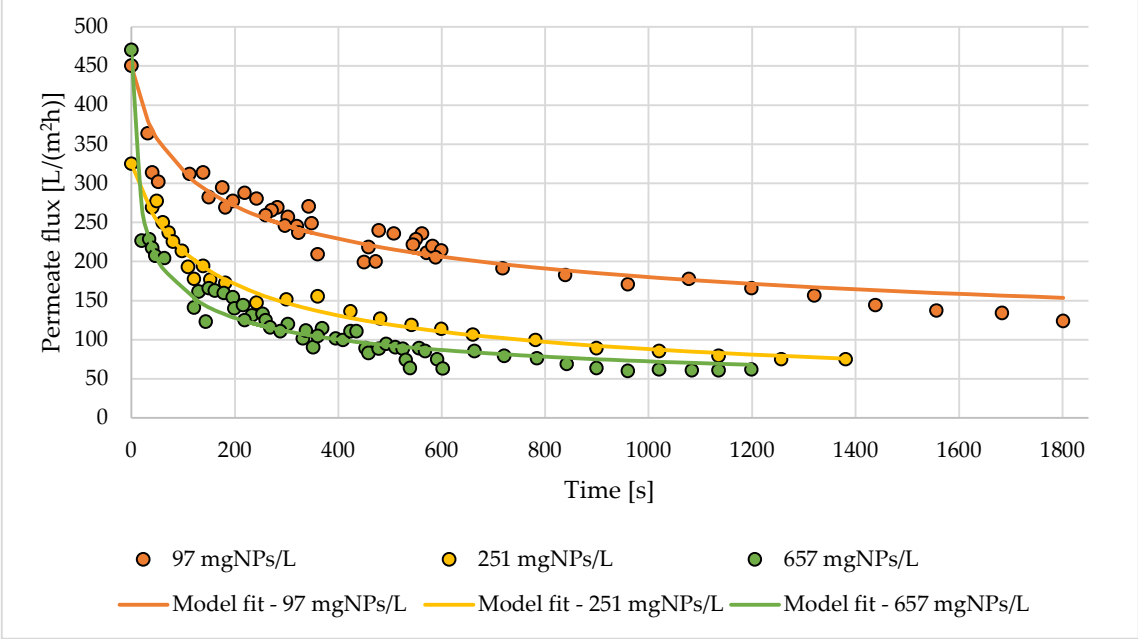

Figure 10. Model fitting for different filtration conditions of nanoparticles in polishing wastewater at 0.4 bar [20]

Preprints (www.preprints.org) | NOT PEER-REVIEWED | Posted: 13 June 2022 doi:10.20944/preprints202206.0187.v1

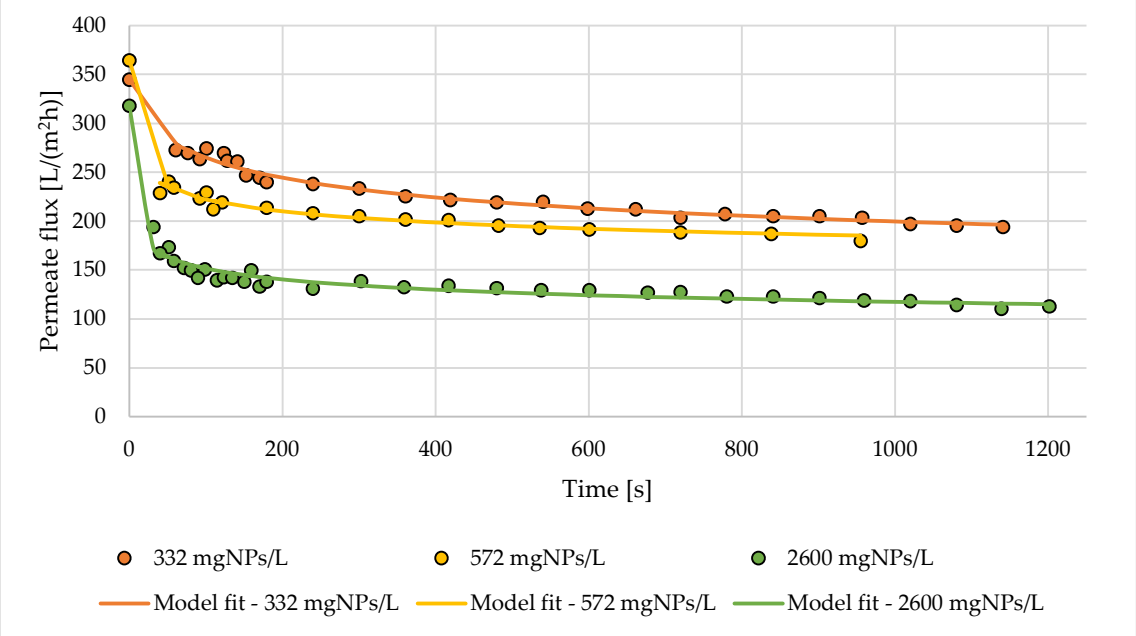

Figure 11. Model fitting for different filtration conditions of nanoparticles in polishing wastewater at 0.3 bar [20]

3.2.2. Applications in Microfiltration

Table 5 displays the fitting data for three different ceramic membranes CM01, CM05 and CM08 used in corn syrup clarification [21]. For the same TMP, the three membranes have different values for k and P. According to [21], the membranes CM01, CM05 and CM08 have hydraulic permeabilities equal to 9.84, 46.63 and 273.45 L/(h.m².kPa), respectively. At constant TMP, as the hydraulic permeability increases, k initially decreases and increases afterwards. The opposite seems to happen to P, as it initially increases and decreases afterwards. As for the use of CM05 at different TMPs, an increase in pressure causes a decrease in k and an increase in P. Therefore, for this membrane in the present case, higher TMPs seem to slow the fouling process. All of the fitting curves can be found in Figures 12 and 13.

Table 5. Model fitting for different filtration conditions of corn syrup clarification [21]

Filtration mechanism	Membrane	TMP (kPa)	k (h^{-1})	P	R^2
Microfiltration	CM08	50	-6.67255	-1.485	0.9837
Microfiltration	CM05	50	-2.48053	-1.251	0.9882
Microfiltration	CM01	50	-11.188	-2.666	0.9621
Microfiltration	CM05	103.42	-3.09844	-1.213	0.9868
Microfiltration	CM05	51.71	-4.47374	-1.614	0.9818
Microfiltration	CM05	37.9	-5.40957	-1.694	0.9936

 doi:10.20944/preprints202206.0187.v1

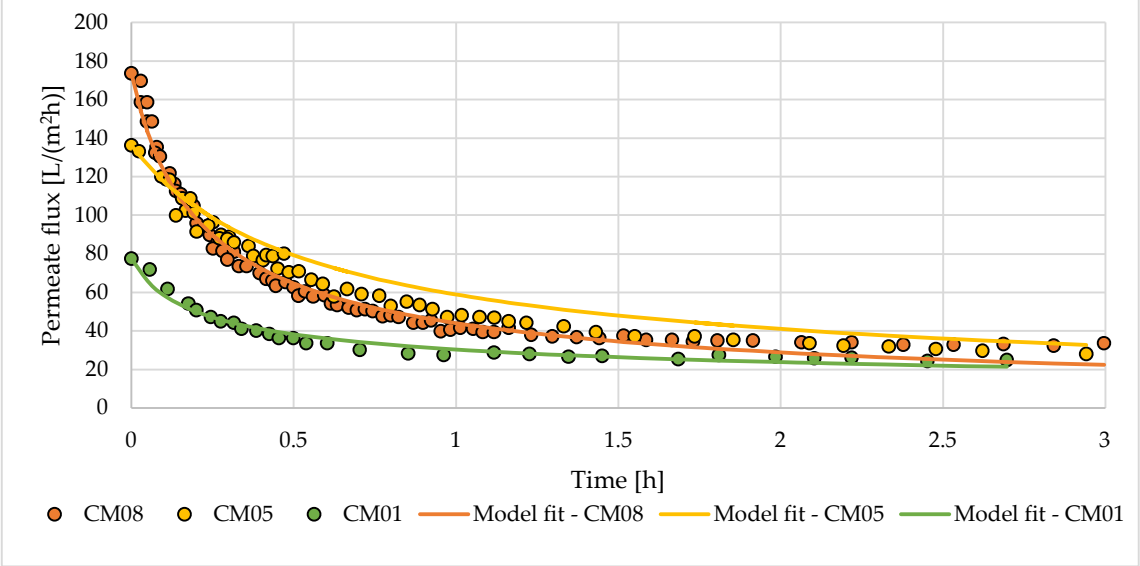

Figure 12. Model fitting for different ceramic membranes in corn syrup clarification [21]

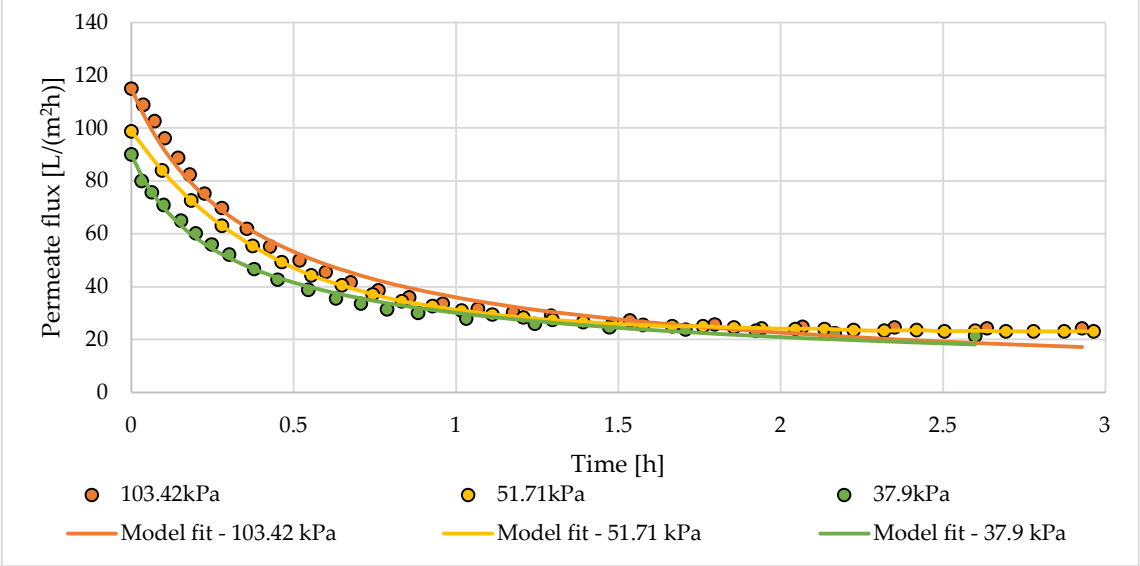

Figure 13. Model fitting for the ceramic membrane CM05 in corn syrup clarification [21]

3.2.3. Applications in Nanofiltration and Reverse Osmosis

According to the data shown in Table 6 and the curves presented in Figures 14 and 15, it is possible to see a correlation between the ionic strength of the solution and k. For both nanofiltration and reverse osmosis, the solution with calcium ions causes an increase in k when compared to the solution with sodium. This increase in k indicates that $j(t)$ decreases more rapidly with a more positively charged solution. For nanofiltration, the values of P do not change drastically with the presence of calcium ions. In contrast, P changes greatly for reverse osmosis.

 doi:10.20944/preprints202206.0187.v1

Table 6. Model fitting for different filtration conditions of humic acid in ionic aqueous solutions [22]

Filtration mechanism	Membrane	Ion	k (min^{-1})	P	R^2
Nanofiltration	NE90	Na^+	-0.00981	-3.736	0.9987
Nanofiltration	NE40	Na^+	-0.01342	-2.441	0.9971
Reverse Osmosis	RE-SHF	Na^+	-8.56E-7	-0.0088	0.9838
Reverse Osmosis	SW30	Na^+	-1.03E-6	-0.0068	0.9633
Nanofiltration	NE90	Ca^{2+}	-0.01656	-2.875	0.9966
Nanofiltration	NE40	Ca^{2+}	-0.02032	-2.494	0.984
Reverse Osmosis	RE-SHF	Ca^{2+}	-0.04657	-7.294	0.988
Reverse Osmosis	SW30	Ca^{2+}	-0.02677	-4.439	0.9677

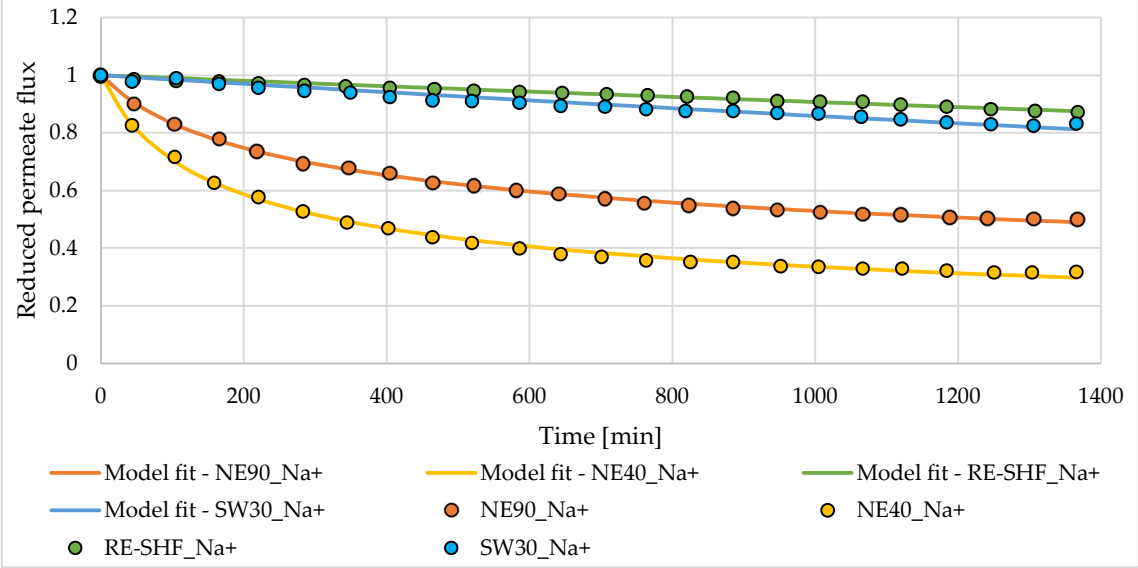

Figure 14. Model fitting for different filtration conditions of humic acid in ionic solutions with Na^+ ions [22]

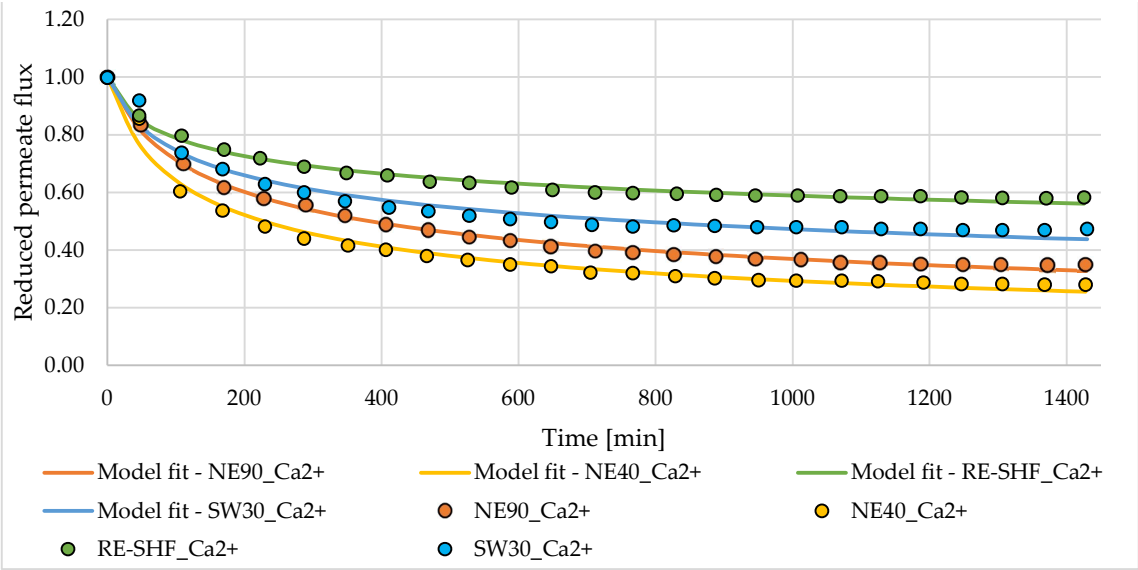

Figure 15. Model fitting for different filtration conditions of humic acid in ionic solutions with Ca^{2+} ions [22]

 doi:10.20944/preprints202206.0187.v1

Table 7 and Figure 16 present how a membrane's composition can influence k and P. [23] originally aimed to study the effects of different percentages of fumarate alumoxane (Fum-A) in the composition could impact fouling. As shown in Table 7, for weight percentages above 1%, both P and k change greatly. For an increase in Fum-A, k tends to increase as the opposite happens to P. Therefore, for greater concentrations of Fum-A, the fouling effect becomes more pronounced.

Table 7. Model fitting for different filtration conditions of whey solutions [23]

Filtration mechanism	Membrane	Fum-A (% w/w)	k (min^{-1})	P	R^2
Nanofiltration	Fum-A/PES	0	-13.08	-4.971	0.9822
Nanofiltration	Fum-A/PES	0.5	-13.05	-4.97	0.9822
Nanofiltration	Fum-A/PES	1	-13.09	-4.971	0.9822
Nanofiltration	Fum-A/PES	2	-1199	-10.23	0.9759
Nanofiltration	Fum-A/PES	3	-1355	-10.23	0.9759

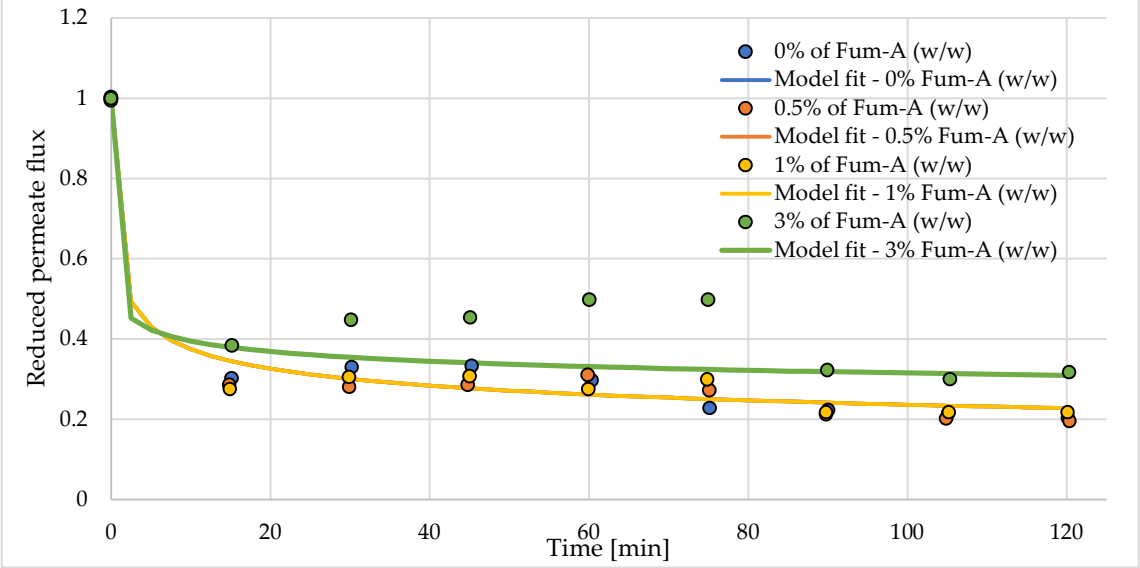

Figure 16. Model fitting for membranes with different Fum-A concentrations and their impact in the filtration of whey solutions [23]

4. Discussion

Taking into account the data in the literature [17], [18], [19], [20], [21], [22] and [23], as well as the model fitting presented in Tables 1-7, it is possible to infer that the effects of variables such as TMP, CFR, filtration mechanism, membrane composition and solution nature vary greatly. The variables that have the biggest impact on the coefficients ***P*** and ***k*** are the membrane composition, the solution nature and the filtration mechanism. As shown in Tables 2 and 3, methods that try to dimmish fouling tend to decrease the value of ***k***. These methods change the membrane composition or the nature of the solution in some way. As demonstrated in Tables 2, 3, 6 and 7, the membrane composition can either increase or decrease ***k***, which depends on the interactions between the solution being filtered and the membrane itself. In general, the effects that TMP, CFR, filtration mechanism, membrane composition and solution nature have on ***P*** and ***k*** are situation-specific. Therefore, to determine these effects, each situation needs to be thoroughly investigated in its own right.

5. Conclusions

- The Hermia model can be used for any real values of n and k for equal or approximate entrance and exit densities;
- The permeate flux j is given by a power law dependent on the value of n for any real $n \neq 2$;
- The permeate flux j is given by an exponential function when $n = 2$;
- The accumulated volume as a function of time follows the same type of ODE expressed by time as a function of the accumulated volume;
- The mass flux $N(t)$ behaves similarly to the permeate flux j;
- There is a correction term for the difference of the entrance and exit densities that scales up j_0 such that the continuity equation is obeyed;
- For $n \neq 2$, j will become a constant value if P tends to infinity;
- P is related to n, since $P = n - 2$;
- Since n is a continuous quantity, there are solutions between the four original discreate values, which can be physically interpreted as the existence of new types of blocking mechanisms;
- The fouling curve $\delta(t)$ is also given by a power law dependent on P for any real $P \neq 0$,
- The fouling curve $\delta(t)$ is also given by an exponential function when $P = 0$,
- When $P \to \infty$, $P \to -\infty$ or $P = -1$, the fouling curves given by $\delta(t)$ behave linearly;
- There is one and only one unique fouling profile $\delta(t)$ for every real value P;
- Ultrafiltration, microfiltration, nanofiltration and reverse osmosis can be modelled;
- The effects of membrane composition and solution nature impact greatly the values of P and k;
- The fouling behavior is situation-specific and P and k may vary differently with the same variable in different cases.

Author Contributions: Gustavo Leite Dias Pereira: Conceptualization, Methodology, Investigation, Writing – Original Draft. **Lucio Cardoso-Filho:** Supervision, Project administration, Resources. **Veeriah Jegatheeesan:** Validation, Writing – Review and Editing. **Reginaldo Guirardello:** Validation, Writing – Review and Editing.

Funding: This research did not receive any financial support or material aid of any kind.

Institutional Review Board Statement: Not applicable.

Data Availability Statement: Not applicable.

Acknowledgments: We thank the State University of Maringa, the State University of Campinas and the RMIT for the help with writing and reviewing the proof.

Conflicts of Interest: The authors declare that they have no known competing financial interests or personal relationships that could have appeared to influence the work reported in this paper.

References

1. Hermia, J. Constant pressure blocking filtration laws—application to power-law non-newtonian fluids, Trans. Inst. Chem. Eng. 60 (1982) 183–187.
2. Vela, M., Blanco, S., García, J. and Rodríguez, E. Analysis of membrane pore blocking models applied to the ultrafiltration of PEG, Separation and Purification Technology 62 (2008) 489–498, doi: 10.1016/j.seppur.2008.02.028
3. Kurada, K., Tanmay and De, S. Modeling of cross flow hollow fiber ultrafiltration for treatment of effluent from Railway Workshop, Journal of Membrane Science 551 (2018) 223–233, doi: 10.1016/j.memsci.2018.01.051
4. Li, S., Luo, J., Hang, X., Zhao, S. and Wan, Y. Removal of polycyclic aromatic hydrocarbons by nanofiltration membranes:

Rejection and fouling mechanisms, Journal of Membrane Science 582 (2019) 264–273, doi: 10.1016/j.memsci.2019.04.008
5. Hwang, K., Liao, C. and Tung, K. Analysis of particle fouling during microfiltration by use of blocking models, Journal of Membrane Science 287 (2007) 287–293, doi:10.1016/j.memsci.2006.11.004
6. Kim, J., Yuan, Y. and Benjamin, M. A serial filtration investigation of membrane fouling by natural organic matter, Journal of Membrane Science 294 (2007) 115–126, doi: 10.1016/j.memsci.2007.02.020
7. Gomes, M., Arroyo, P. and Pereira, N. Biodiesel production from degummed soybean oil and glycerol removal using ceramic membrane, Journal of Membrane Science 378 (2011) 453–461, doi: 10.1016/j.memsci.2011.05.033
8. Gomes, M., Arroyo, P. and Pereira, N. Influence of acidified water addition on the biodiesel and glycerol separation through membrane technology, Journal of Membrane Science 431 (2013) 28–36, doi: 10.1016/j.memsci.2012.12.036
9. Chang, E., Yang, S., Huang, C., Liang, C. and Chiang, P. Assessing the fouling mechanisms of high-pressure nanofiltration membrane using the modified Hermia model and the resistance-in-series model, Separation and Purification Technology 79 (2011) 329–336, doi: 10.1016/j.seppur.2011.03.017
10. Hasyimah, M. and Mohammad, A. Assessment of Fouling Mechanisms in Treating Organic Solutes Synthesizing Glycerin−Water Solutions by Modified Hermia Model, Industrial and Engineering Chemistry Research 53 (2014) 15213−15221, doi: 10.1021/ie502509d
11. Pan, Y., Wang, W., Wang, T. and Yao, P. Fabrication of carbon membrane and microfiltration of oil-in-water emulsion: An investigation on fouling mechanisms, Separation and Purification Technology 57 (2007) 388–393, doi: 10.1016/j.seppur.2007.04.024
12. Çengel, Y. and Cimbala, J. Fluid Mechanics: Fundamentals and Applications, 1st Edition by McGraw-Hill Higher Education. ISBN: 0-07-247236-7.
13. Welty, J., Rorrer, G. and Foster, D. Fundamentals of Momentum, Heat, and Mass Transfer, 6th Edition by John Wiley & Sons, Inc. ISBN: 978-0-470-50481-9.
14. Magyar, P. Derivative of Inverse Functions, Lecture notes. Available at [https://users.math.msu.edu/users/magyarp/]. Accessed at 11/06/2021.
15. Protter, M., Morrey, C. Intermediate Calculus: Differentiation under the Integral Sign, 2nd Edition by Springer. ISBN: 978-0-387-96058-6.
16. Ricardo, H. A Modern Introduction to Differential Equations, 3rd Edition by Elsevier Academic Press. ISBN 978-0128234174.
17. Kurada, K. and Tanmay, S. Modeling of cross flow hollow fiber ultrafiltration for treatment of effluent from Railway Workshop, Journal of Membrane Science 551 (2018) 223-233, doi: 10.1016/j.memsci.2018.01.051
18. Jung, C. and Son, H. Evaluation of membrane fouling mechanism in various membrane pretreatment processes, Desalination and Water Treatment, 2:1-3, 199-208, doi: 10.5004/dwt.2009.256
19. Storms, M., Kadhem, A., Xiang, S., Bernards, M., Gentile, G. and Cortalezzi, M. Enhancement of the fouling resistance of zwitterion coated ceramic membranes, Membranes 2020, 10, 210, doi: 10.3390/membranes10090210
20. Ohanessian, K., Monnot, M., Moulin, P., Ferrasse, J., Barca, C., Soric, A. and Boutin, O. Dead-end and crossflow ultrafiltration process modelling: application on chemical mechanical polishing wastewaters, Chemical Engineering Research and Design, 2020, 158, 164-176, doi: 10.1016/j.cherd.2020.04.007
21. Almandoz, C., Pagliero, C., Ochoa, A. and Marchese, J. Corn syrup clarification by microfiltration with ceramic membranes, Journal of Membrane Science 363 (2010) 87-95, doi: 10.1016/j.memsci.2010.07.017
22. Park, J., Jeong, K., Baek, S., Park, S., Ligaray, M., Chong, T. and Cho, K. Modeling of NF/RO membrane fouling and flux decline using reeal-time observations, Journal of Membrane Science 576 (2019) 66-77, doi: 10.1016/j.memsci.2019.01.031
23. Heidari, S., Amirinejad, M. and Jahangirian, H. Investigation of fouling mechanisms using surface morphology and physicochemical membrane features, Chemical Engineering Technology 2019, 42, No. 6, 1310-1320, doi: 10.1002/ceat.201800635